Available online at www.sciencedirect.com
ScienceDirect
Nuclear Instruments and Methods in Physics Research A 581 (2007) 799–815
NUCLEAR INSTRUMENTS & METHODS IN PHYSICS RESEARCH Section A
www.elsevier.com/locate/nima

Beam matching adaptive control via extremum seeking ☆

Eugenio Schuster[a,*], Chao Xu[a], Nicholas Torres[a], Eiji Morinaga[d], Christopher Allen[b], Miroslav Krstic[c]

[a]Department of Mechanical Engineering and Mechanics, Lehigh University, 19 Memorial Drive West, Bethlehem, PA 18015 0385, USA
[b]Los Alamos National Laboratory, Los Alamos, NM 87545, USA
[c]Department of Mechanical and Aerospace Engineering, University of California at San Diego, 9500 Gilman Dr., La Jolla, CA 92093 0411, USA
[d]Department of Computer-Controlled Mechanical Systems, Osaka University, 2-1 Yamadaoka, Suita, Osaka 565-0871, Japan

Received 9 January 2007; received in revised form 18 July 2007; accepted 26 July 2007
Available online 12 August 2007

Abstract

The matching problem for a low energy transport system in a charged particle accelerator is approached using the extremum seeking method for non-model based optimization and adaptive control. The beam dynamics used for numerical simulations are given by the KV (Kapchinsky–Vladimirsky) envelope equations. Extremum seeking is employed for the lens tuning in both a matching and a periodic channel. Numerical simulations illustrate the effectiveness of this approach.

PACS: 29.27.−a; 29.27.Eg; 02.30.Yy; 41.85.Lc

Keywords: Beam matching; Adaptive control

1. Introduction

In the design of a particle accelerator, feedback control systems are becoming an essential part of the system. The uses of control are numerous: from the magnet power supplies, to RF systems, to various control loops dedicated to certain properties of the beam (steering, phase and position in storage rings, etc.). In this work we approach the beam matching problem, where the beam must be matched to the acceptance ellipse of an accelerating structure or transport section. Specifically, we consider a fixed-geometry matching section consisting of n quadrupole lenses. The objective of this system is to take any arbitrary initial beam state (phase coordinates) and "match" it to the acceptance ellipse of the following section, i.e., any given initial state x_{ini} to a prescribed target state x_{tar} at one or more locations along the channel, through the control of the lens focusing strengths in the matching channel. We also consider that the matching section may be followed by a fixed-geometry periodic section, where initial and final states are identical (x_{p}). A review of beam transport including matching was recently presented in Ref. [1]. Envelope matching of electron beams in a fixed lattice of short magnets was also studied in Ref. [2].

We assume the matching channel to be composed of discrete beamline elements, such as lenses, and drifts. These elements are cascaded along the beam axis, labeled as the z axis, to form the transport channel. The matching channel configuration is depicted in Fig. 1a. The inputs to the lenses, labeled θ_i, for $i = 1 \ldots n$, represent the focusing strengths of the lenses and are the parameters of the matching channel that may be varied. The periodic channel configuration is depicted in Fig. 1b. The focusing function in this channel must be symmetric, i.e., the absolute values of the lens focusing strengths must be identical and equal to θ_{p}. This common lens strength is the parameter of the periodic channel that may be varied.

☆This work was supported in part by a grant from the Commonwealth of Pennsylvania, Department of Community and Economic Development, through the Pennsylvania Infrastructure Technology Alliance (PITA), and in part by the NSF CAREER award program (ECCS-0645086).
*Corresponding author.
E-mail address: schuster@lehigh.edu (E. Schuster).

0168-9002/$ - see front matter © 2007 Elsevier B.V. All rights reserved.
doi:10.1016/j.nima.2007.07.154

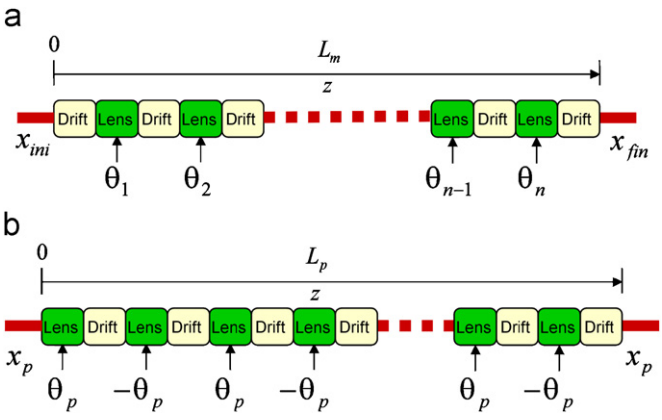

Fig. 1. (a) Matching and (b) periodic channels.

The design of particle beam matching systems has been originally accomplished by an iterative procedure, where the beam is simulated in a given transport system, and the knobs of the lens focusing strengths are continually adjusted until a satisfactory solution is obtained. There has been some effort on automating this procedure, and several codes based on model-based optimization techniques are available to find a matching solution off-line. As a mode of example, in Ref. [3] the problem was approached from a control theoretical point of view, using local (nonlinear programming) and global (dynamic programming) optimal control methods, and based on a multistage control network model. The global method is practical only for axisymmetric systems. It has been shown to become too computationally intensive for particle beams with more degrees of freedom. For these beams, the local method is substantially faster at the expense of finding local minima of the cost functional, which may not be the best (global) solution.

The major shortcoming of these model-based methods is their dependence on the model. The accuracy of the calculation is limited by the uncertainties associated with the initial beam conditions, magnet modeling, exact beam current, emittances, magnet locations, etc. Therefore, the implementation of the calculated element strengths in a real experiment does not yield true matching conditions. Under these circumstances, the "knobs" for the lens focusing strengths must be adjusted on-line. The success of such a procedure relies at present completely upon the experience, judgement, and intuition of the operator.

In this paper we introduce extremum seeking as an effective optimization technique to find an optimal matching solution both on-line (real-time experiment) and off-line (simulated environment) for a four-quadrupole or six-quadrupole matching channel. By optimal matching solution we understand a set of lens focusing strengths which minimizes a cost function that measures the "error" between the actual beam envelope trajectory and the target or desired beam envelope trajectory, i.e., that measures the degree of matching. The target or desired trajectory is provided by the designer based on requirements on beam envelope excursions and emittance growth [4]. Due to its non-model-based nature, extremum seeking is well suited to overcome the limitations described above for model-based optimization methods in terms of uncertainty handling. Therefore, a hybrid scheme is also presented in this paper, where the optimal lens focusing strengths are computed off-line using either extremum seeking (Section 4) or another model-based optimization technique, and used as initial conditions for an on-line, extremum-seeking controller (Section 5). Under this framework, the extremum seeking algorithm plays the role of a non-model-based, adaptive controller, which is one of its unique characteristics, ensuring a well-matched beam independently of uncertainties or changes in the system parameters.

The paper is organized as follows. In Section 2 the control problem is defined. Section 3 introduces the fundamentals of extremum seeking. The effectiveness of the extremum seeking algorithm for beam matching optimization is demonstrated in Section 4 through an extensive numerical study. The possible use of extremum seeking as an adaptive controller is illustrated in Section 5 and represents a major contribution of this technique to particle accelerator operation. In this case, the initial tuning of the lens strengths, computed off-line by a model-based optimization technique, is "corrected" in real time by the extremum seeking adaptive controller to compensate for unmodeled effects such as fluctuations in the initial conditions of the beam, uncertainties or changes in the physical characteristics of the beam, and faults, drifts or hysteresis of the actuators (electromagnetic lenses). Therefore, the extremum seeking adaptive controller makes the channel robust against these effects, and a well-matched beam is achieved for any condition of the beam and the channel. The paper is closed by a summary in Section 6.

2. Problem definition

Assuming a continuous, elliptically symmetric particle beam, we model its dynamics using the KV (Kapchinsky–Vladimirsky) coupled-envelope equations [5]. Let the z coordinate represent the position along the design trajectory, and thus the x–y plane is the transverse plane for the particle beam. At each z location, let $X(z)$ and $Y(z)$ represent the dimension of the semi-axes of the beam envelope in the x and y planes, respectively. We refer to $X(z)$ and $Y(z)$ as the beam envelope trajectory. The KV equations then appear as

$$X'' - \theta(z)X - \frac{2K}{X+Y} - \frac{\varepsilon_X^2}{X^3} = 0 \tag{1}$$

$$Y'' + \theta(z)Y - \frac{2K}{X+Y} - \frac{\varepsilon_Y^2}{Y^3} = 0 \tag{2}$$

where the prime indicates differentiation with respect to z, which plays the role of "time" in an optimal control framework. K is the beam perveance [6], ε_X and ε_Y are the effective unnormalized emittances of the beam in the x and

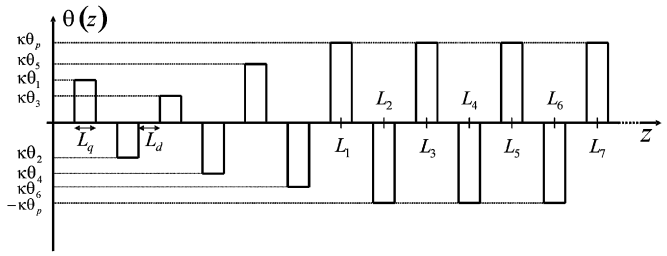

Fig. 2. Focusing function $\theta(z)$ for a six-quadrupole matching channel followed by a periodic channel, where κ is a constant, θ_i, for $i = 1, \ldots, 6, p$ in this example, represents the focusing strengths of the lenses (control inputs), L_d is the drift length, and L_q is the quadrupole effective lens length. L_i, for $i = 1, \ldots, 7$ in this example, represents the center positions of the quadrupole lenses in the periodic channel.

y planes, respectively. The function $\theta(z)$, shown in Fig. 2 for a six-quadrupole matching channel followed by a periodic channel, is the focusing (control) function; κ is a constant, L_d is the drift length, and L_q is the quadrupole effective lens length. The physical parameters used in the simulations presented in this paper, and chosen arbitrarily with the only purpose of illustrating the effectiveness of the extremum seeking approach to beam matching, are $K = 2.7932 \times 10^{-6}\,\mathrm{rad}^2$, $\varepsilon_X = 6 \times 10^{-6}\,\mathrm{m\,rad}$, $\varepsilon_Y = 6 \times 10^{-6}\,\mathrm{m\,rad}$, $\kappa = 2.6689$ (see Fig. 2), $L_d = 0.1488\,\mathrm{m}$, $L_q = 0.0610\,\mathrm{m}$. The n-lens matching channel parameters (lens strengths) must satisfy the following constraints:

$$|\theta_i| \leqslant \bar{\theta} \quad \text{for } i = 1, \ldots, n$$
$$\theta_j \geqslant 0 \quad \text{for } j = \text{odd}$$
$$\theta_k \leqslant 0 \quad \text{for } k = \text{even}$$

while the periodic channel parameter must satisfy

$$0 \leqslant \theta_p \leqslant \bar{\theta}.$$

For simulation purposes, $\bar{\theta} = 50$ has been considered in this paper.

We are given initial conditions for the beam at $z = 0$, the transport system's entrance location. These conditions characterize the beam coming from the preceding section of the transport or accelerator system. They may be translated into initial conditions for the beam envelopes in the x plane (X_{ini}, X'_{ini}) and in the y plane (Y_{ini}, Y'_{ini}). In matching systems we are also given desired target conditions at specific locations along the axis, for instance, at $z = L_m$, the exit location of the matching channel (see Fig. 1a). We denote these target conditions as (X_{tar}, X'_{tar}) and (Y_{tar}, Y'_{tar}). They may be prescribed by the acceptance requirements of the next section of the transport or accelerator system.

Denoting $x = [X \;\; X' \;\; Y \;\; Y']^{\mathrm{T}}$, we define

$$x_{\mathrm{ini}} = x(0) = \begin{bmatrix} X_{\mathrm{ini}} \\ X'_{\mathrm{ini}} \\ Y_{\mathrm{ini}} \\ Y'_{\mathrm{ini}} \end{bmatrix}, \quad x_{\mathrm{tar}} = \begin{bmatrix} X_{\mathrm{tar}} \\ X'_{\mathrm{tar}} \\ Y_{\mathrm{tar}} \\ Y'_{\mathrm{tar}} \end{bmatrix}. \tag{3}$$

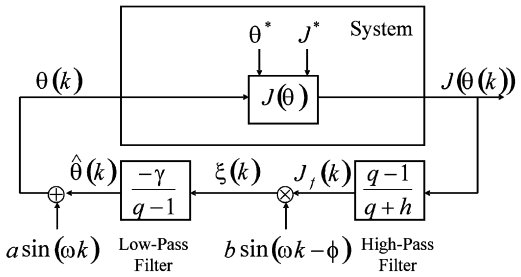

Fig. 3. Extremum seeking control scheme.

In addition, we define desired beam envelope trajectories for $X(z)$ and $Y(z)$ denoted as $X_{\mathrm{des}}(z)$ and $Y_{\mathrm{des}}(z)$, respectively. Some examples of how to choose such trajectories will be given for some of our study cases later in the paper. Given x_{ini}, x_{tar}, $X_{\mathrm{des}}(z)$ and $Y_{\mathrm{des}}(z)$, we use an extremum seeking procedure to minimize (maximize) a cost function $J = J(x, x_{\mathrm{tar}}, X_{\mathrm{des}}(z), Y_{\mathrm{des}}(z))$, which is a direct measure of mismatching (matching). The problem is formulated as finite-"time" optimal control ($0 \leqslant z \leqslant L$), with bang–bang controls[1] of fixed durations but varying intensities (i.e., with a very coarse discretization in "time" which results in a highly constrained waveform for the control $\theta(z)$ as it is shown in Fig. 2), for a plant that is nonlinear. This is far from being a standard optimization problem. To add complexity to the problem, we are seeking robustness against uncertainties of the system for a successful practical implementation of the control method.

3. Extremum seeking

Extremum seeking control, a popular tool in control applications in the 1940–1950s, has seen a resurgence in popularity as a real time optimization tool in different fields of engineering [7–9]. Aerospace and propulsion problems (formation flight [10]), combustion instabilities [11,12], flow control [13,14], compressor rotating stall [15], automotive problems (soft landing of electromagnetic valves [16]), heat transfer problems [17], and bioreactors [18] are among its applications. Extremum seeking is applicable in situations where there is a nonlinearity in the control problem, and the nonlinearity has a local minimum or a maximum. The parameter space can be multidimensional. In this paper we use extremum seeking for iterative optimization of the lens focusing strengths θ_i, for $i = 1, \ldots, n$, and eventually θ_p, to make x as close as possible to x_{tar} at prescribed locations along the channel. We point out that, since x_{tar} is given arbitrarily, x is obtained via solving a system of nonlinear differential equations, and the lens input applied through $\theta(z)$ is highly constrained in its waveform (Fig. 2), there may not exist a set of lens focusing strengths for which *perfect* matching is

[1] It is sometimes the case that a control is restricted to be between a lower and an upper bound. If the control switches from one extreme to the other at certain times (i.e., the control is never strictly in between the bounds) then the control is referred to as a bang–bang control.

achieved ($J=0$), thus we try to obtain the best possible *approximate* matching ($J=$ minimum).

We change the lens focusing strengths after each beam "run" (extremum seeking iteration). Thus, we employ the discrete-time version [19] of extremum seeking. The implementation is depicted in Fig. 3, where q denotes the variable of the Z-transform [20]. The Z-transform plays the same role in discrete-time systems that the Laplace transform [21] plays in analysis of continuous-time systems. Given a sequence $u_0, u_1, \ldots, u_k, \ldots$, denoted as $\{u(k)\}$, and where k denotes the discrete time, its Z-transform is defined as

$$\mathscr{Z}\{u(k)\} = U(q) = \sum_{k=-\infty}^{k=\infty} u_k q^{-k}. \tag{4}$$

From this definition it is possible to note that

$$\mathscr{Z}\{u(k+1)\} = qU(q), \quad \mathscr{Z}\{u(k-1)\} = q^{-1}U(q) \tag{5}$$

for which q is also called the time shift operator. The Z-transform permits the rapid conversion of a linear, constant-coefficient, difference equation in the discrete-time domain into a transfer function in the Z-domain, which is defined as the ratio of the Z-transform of the system output to the Z-transform of the system input. Therefore, the dynamics of a discrete-time linear system can be expressed either by a difference equation in the discrete-time domain or by a transfer function in the Z-domain.

The high-pass filter in Fig. 3 is designed as $0<h<1$, and the modulation frequency ω is selected such that $\omega=\alpha\pi$, $0<|\alpha|<1$, and α is rational. The static nonlinear block $J(\theta)$ is defined to be a measure of the matching error. The objective is to minimize J. We present next an elementary intuitive explanation of how the scheme works. A rigorous analysis can be found in Refs. [9,19].

Without loss of generality, the static nonlinear block $J(\theta)$ is assumed to have a minimum at $\theta=\theta^*$, and to be of the form

$$J(\theta) = J^* + \frac{J''}{2}(\theta-\theta^*)^2 \tag{6}$$

where $J''>0$. Any C^2 function, $J(\theta)$, can be approximated locally by Eq. (6). The purpose of the extremum seeking algorithm is to make $\theta-\theta^*$ as small as possible, so that the output $J(\theta)$ is driven to its minimum J^*. The probing signal $a\sin(\omega t)$, with $a>0$, fed into the plant helps to get a measure of gradient information of the map $J(\theta)$. We note that $\hat{\theta}$ in Fig. 3 denotes the estimate of the unknown optimal input θ^*. Let

$$\tilde{\theta} = \theta^* - \hat{\theta} \tag{7}$$

denote the estimation error. Thus,

$$\theta(k) - \theta^* = a\sin(\omega k) - \tilde{\theta}(k) \tag{8}$$

which, when substituted into Eq. (6), gives

$$J(k) \equiv J(\theta(k)) = J^* + \frac{J''}{2}(\tilde{\theta}(k) - a\sin(\omega k))^2. \tag{9}$$

Taking into account the trigonometric identity $2\sin^2(\omega k) = 1-\cos(2\omega k)$, we can rewrite Eq. (9) as

$$J(k) = J^* + \frac{a^2J''}{4} + \frac{J''}{2}\tilde{\theta}(k)^2 - aJ''\tilde{\theta}(k)\sin(\omega k) - \frac{a^2J''}{4}\cos(2\omega k). \tag{10}$$

The high-pass filter, applied to $J(k)$, will remove the constant terms and generate the signal

$$J_f(k) = \frac{J''}{2}\tilde{\theta}(k)^2 - aJ''\tilde{\theta}(k)\sin(\omega k) - \frac{a^2J''}{4}\cos(2\omega k)$$

which is in turn demodulated by being multiplied by $b\sin(\omega k-\phi)$, with $b>0$, to generate

$$\xi(k) = \frac{bJ''}{2}\tilde{\theta}(k)^2\sin(\omega k) - abJ''\tilde{\theta}(k)\sin^2(\omega k) - \frac{a^2bJ''}{4}\cos(2\omega k)\sin(\omega k) \tag{11}$$

where we have taken $\phi=0$ to simplify the analysis. Applying again $2\sin^2(\omega k) = 1-\cos(2\omega k)$, as well as the trigonometric identity $2\cos(2\omega k)\sin(\omega k) = \sin(3\omega k) - \sin(\omega k)$, we can rewrite (11) as

$$\xi(k) = -\frac{abJ''}{2}\tilde{\theta}(k) + \frac{abJ''}{2}\cos(2\omega k) + \frac{a^2bJ''}{8}(\sin(\omega k) - \sin(3\omega k)) + \frac{bJ''}{2}\tilde{\theta}(k)^2\sin(\omega k). \tag{12}$$

The low-pass filter ($\gamma>0$), applied to $\xi(k)$, will remove the high-frequency terms (last three terms). Therefore, we can write

$$\hat{\theta}(k) = \frac{-\gamma}{q-1}\xi(k) \approx \frac{\gamma}{q-1}\frac{abJ''}{2}\tilde{\theta}(k). \tag{13}$$

Taking into account definition (5) for the shift operator q, we can write

$$\hat{\theta}(k+1) - \hat{\theta}(k) = \gamma\frac{abJ''}{2}\tilde{\theta}(k). \tag{14}$$

We note that $\hat{\theta}(k+1) - \hat{\theta}(k) = -(\tilde{\theta}(k+1) - \tilde{\theta}(k))$, and write

$$\tilde{\theta}(k+1) = \tilde{\theta}(k) - \gamma\frac{abJ''}{2}\tilde{\theta}(k) = \left(1-\gamma\frac{abJ''}{2}\right)\tilde{\theta}(k). \tag{15}$$

Provided that $|1-\gamma(abJ''/2)|<1$ (a, b, and γ are design parameters), this is a stable system. Thus, $\tilde{\theta}\to 0$, i.e., $\hat{\theta}\to\theta^*$.

Looking back at our elementary intuitive analysis, it is important to note that the approximations hold only when ω is large in a qualitative sense. The cut-off frequencies of the filters need to be lower than the frequency ω of the perturbation signal. These observations impose constraints and, at the same time, a relationship on ω and h. As an additional constraint, ω should not equal any frequency present in the measurement noise. The perturbation

amplitude a needs to be small in order to make the steady state output error also small. Given a and b, the adaptation gain γ needs to be small enough to satisfy the stability condition $|1-\gamma(abJ''/2)|<1$.

In this case, we are dealing with a multi-parameter extremum seeking procedure (the number of parameters n_p considered in the following sections will be 4, 6 or 7). Thus, we write

$$\theta(k)=\begin{bmatrix}\theta_1(k)\\ \vdots \\ \theta_{n_p}(k)\end{bmatrix},\quad \hat{\theta}(k)=\begin{bmatrix}\hat{\theta}_1(k)\\ \vdots \\ \hat{\theta}_{n_p}(k)\end{bmatrix},\quad \xi(k)=\begin{bmatrix}\xi_1(k)\\ \vdots \\ \xi_{n_p}(k)\end{bmatrix}. \tag{16}$$

The extremum seeking constants shown in Fig. 3 are written as $a=b=\mathrm{diag}([a_1\ \cdots\ a_{n_p}])$, and $\gamma=\mathrm{diag}([\gamma_1\ \cdots\ \gamma_{n_p}])$. In addition, we use the special compact notation where $\sin(\omega k-\phi)$ is a vector which denotes

$$\sin(\omega k-\phi)=\begin{bmatrix}\sin(\omega_1 k-\phi_1)\\ \vdots \\ \sin(\omega_{n_p} k-\phi_{n_p})\end{bmatrix}. \tag{17}$$

It is convenient to use a separate frequency for each parameter tracking loop, following the guidelines given above. In general, using a single frequency to excite multiple parameter tracking loops leads to a greater coupling, and consequently to an increase of the design difficulty.

In a simulation environment (model-based extremum seeking), we understand by "run" the integration of the KV equations. In each iteration of the extremum seeking procedure, $\theta(k)$ contains the lens focusing strengths θ_i, for $i=1,\ldots,n$, and eventually θ_p, and is used to compute the focusing function $\theta(z)$, shown in Fig. 2. This function is in turn fed into the model given by the KV equations (1) and (2). Given x_{ini}, the KV equations are integrated to obtain $X(z)$, $Y(z)$, which are necessary to evaluate the cost function, $J(k)=J(\theta(k))$. In a real experiment (non-model-based extremum seeking), we understand by "run" one measure of the beam envelope. In this case, X and Y at the prescribed locations are direct measures. As the sensor technology evolves, and some concepts under investigation such as fluorescent-gas-based sensors become a reality, we may reach the ideal situation where one "run" is coincident with one pulse of the accelerator, i.e., the passage of one beam bunch through the envelope sensors located at prescribed locations. Present sensor technology (e.g., wire scanners or laser scanners) may not be as fast. However, this does not represent a limitation for an extremum seeking implementation. It only implies longer convergence times because the real time between extremum seeking iterations is governed by the speed of the envelope sensors.

The output of the nonlinear static map, $J(k)=J(\theta(k))$, is then used to compute $\theta(k+1)$ according to the extremum seeking procedure in Fig. 3, or written equivalently as

$$J_f(k)=-hJ_f(k-1)+J(k)-J(k-1) \tag{18}$$

$$\xi(k)=J_f(k)b\sin(\omega k-\phi) \tag{19}$$

$$\hat{\theta}(k+1)=\hat{\theta}(k)-\gamma\xi(k) \tag{20}$$

$$\theta(k+1)=\hat{\theta}(k+1)+a\sin(\omega(k+1)). \tag{21}$$

Note that Eqs. (18) and (21) are the difference-equation versions of the transfer functions for the high-pass and low-pass filters in Fig. 3.

The extremum seeking parameters used in all the simulations presented in this paper are $h=0.4$, $\omega_i=\omega_{base}^i\times\pi$, $\gamma_i=0.1(M(\omega_1)/M(\omega_i))$, and $\phi_i=-\phi(\omega_i)$ for $i=1,\ldots,n_p$, where $\omega_{base}=0.95$, and $M(\omega)$ and $\phi(\omega)$ are, respectively, the magnitude and phase of the frequency response of the high-pass filter in Fig. 3.

4. Optimal beam matching

Given x_{ini}, x_{tar}, $X_{des}(z)$ and $Y_{des}(z)$, we use an extremum seeking procedure to find the lens strengths ($\theta=[\theta_1\ \ \theta_2\ \ \theta_3\ \ \theta_4]^T$) of a four-quadrupole matching channel which minimize the cost function J given by

$$J=\{k_1J_1+k_2J_2+k_3J_3\}^{1/2} \tag{22}$$

$$J_1=K_X(x(L_m)-X_{tar})^2+K_Y(Y(L_m)-Y_{tar})^2 \tag{23}$$

$$J_2=K_X^{der}(X'(L_m)-X'_{tar})^2+K_Y^{der}(Y'(L_m)-Y'_{tar})^2 \tag{24}$$

$$J_3=\int_0^L w(z)[K_X^{int}(X(z)-X_{des}(z))^2+K_Y^{int}(Y(z)-Y_{des}(z))^2]\,dz \tag{25}$$

where k_1, k_2, k_3, K_X, K_Y, K_X^{der}, K_Y^{der}, K_X^{int}, and K_Y^{int} are weight constants, and w_z is an integral weight function. The first component of the cost function (22), J_1, measures the mismatching for the semi-axes of the beam envelope at the exit of the matching channel. The second component J_2 measures the mismatching for the derivatives of the semi-axes of the beam envelope at the exit of the matching channel. Finally, the third component J_3 measures the weighted mismatching for the trajectories of the semi-axes of the beam envelope within the matching channel.

We start considering the following initial (entrance of the channel) and target conditions:

$$x_{ini}=\begin{bmatrix}0.001474\\ -0.006013\\ 0.002014\\ 0.007686\end{bmatrix},\quad x_{tar}=\begin{bmatrix}0.001094\\ -0.007865\\ 0.003290\\ 0.011726\end{bmatrix}, \tag{26}$$

where the target condition is specified at the exit of the matching channel, i.e., at $z=L_m$ (see Fig. 1). This pair of initial and target conditions has been carefully chosen to make $\theta=[38\ \ -38\ \ 38\ \ -38]^T$ the unique solution (global minimum) of our matching problem. Knowing the solution of the matching problem beforehand allows us to assess the effectiveness of the extremum seeking algorithm. The initial

conditions for the extremum seeking parameters are $\theta_1(0) = \theta_3(0) = 25$, and $\theta_2(0) = \theta_4(0) = -25$.

Terminal constraints only: Figs. 4 and 5 show the extremum seeking results when the cost function parameters are given by

$$K_X = 2000, \quad K_Y = 1000, \quad K_X^{\text{der}} = 0, \quad K_Y^{\text{der}} = 0$$
$$K_X^{\text{int}} = K_Y^{\text{int}} = 0, \quad k_1 = 1, \quad k_2 = 0, \quad k_3 = 0. \tag{27}$$

The converged value of θ, and its associated state at $z = L_{\text{m}}$, are

$$\hat{\theta}_{\text{conv}} = \begin{bmatrix} 28.0635 \\ -33.4561 \\ 23.7620 \\ -34.4235 \end{bmatrix}, \quad x(L_{\text{m}}) = \begin{bmatrix} 0.001091 \\ -0.007151 \\ 0.003294 \\ 0.007128 \end{bmatrix}. \tag{28}$$

Comparing $x(L_{\text{m}})$ with x_{tar}, we can note that we have very good matching for X and Y, which was our goal ($k_2 = k_3 = 0$). However, although the matching for X' is probably acceptable, the matching for Y' is not. Fig. 4c shows the beam envelope as a function of z (beam envelope trajectory) for $\theta = \hat{\theta}_{\text{conv}}$. The time evolution of $\theta_1, \theta_2, \theta_3, \theta_4$ in Fig. 4b shows a fast convergence. We can see that after 100 iteration we arrive at what we can consider a steady state situation. This fast convergence can be also noted looking at the evolution of the cost function in Fig. 4a.

In all the cases presented in this paper, convergence is analyzed based on the number of "runs" or extremum seeking "iterations." Although the duration of a "run" in a simulated (off-line, model-based extremum seeking) environment is very short because the integration of the KV equations can be carried out very fast using modern computers, the duration of a "run" in a real-time (on-line, non-model-based extremum seeking) experiment can be significant and depends on the sensor technology employed. As already discussed in Section 3, the duration of a "run" in a real-time experiment, or the elapsed time between extremum seeking iterations, and therefore the convergence time, will depend on the sensor speed, i.e., the time required by the sensor to produce two consecutive measurements.

The complexity of the problem is evident from Fig. 5, where the cost function is plotted as a function of $\theta_1, \theta_2, \theta_3, \theta_4$. Each combination of θ_i's, for $i = 1, 2, 3, 4$, defines a case. In Fig. 5a, $|\theta_i|$, for $i = 1, 2, 3, 4$, is varied from 0 to 50 in steps of 5. In Fig. 5b, $|\theta_i|$, for $i = 1, 2, 3, 4$, is varied from 35 to 41 in steps of 1. The negative peak corresponds to $\theta = [38 \quad -38 \quad 38 \quad -38]^{\text{T}}$, which constitutes the global minimum. In Fig. 5c, θ_1 is varied from 27.8 to 28.3, θ_2 is varied from -33.2 to -33.7, θ_3 is varied from 23.5 to 24, θ_4 is varied from -34.2 to -34.7 in steps of 0.1. The converged value $\hat{\theta}_{\text{conv}}$ in Eq. (28) is then just a local

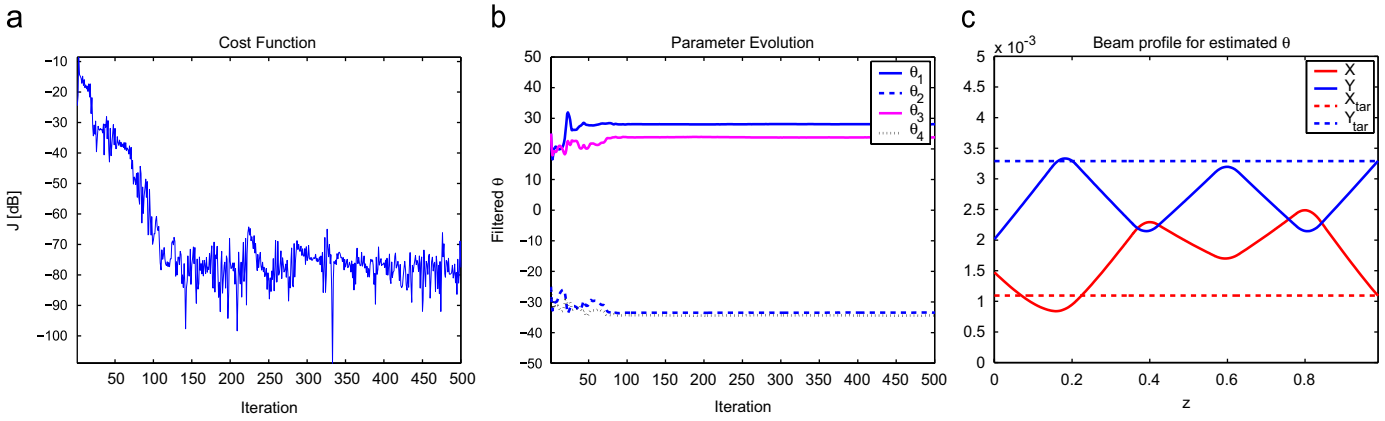

Fig. 4. (a) Cost function evolution, (b) θ evolution, and (c) beam envelope trajectory for $\theta = \hat{\theta}_{\text{conv}}$.

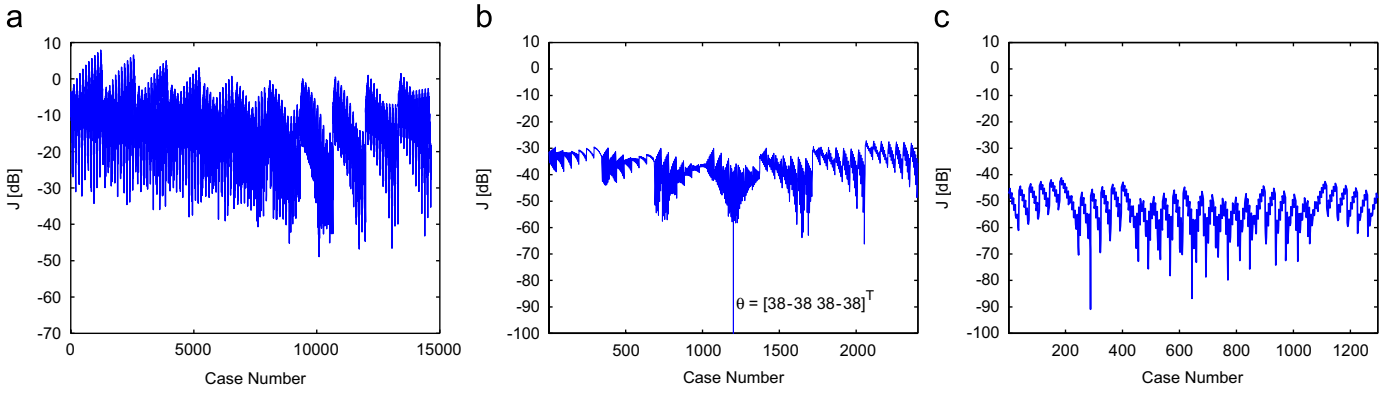

Fig. 5. Cost function map for different combinations of $\theta_1, \theta_2, \theta_3, \theta_4$.

minimum, similar to those shown in this last figure. The converged value cannot be marked in Fig. 5c because it is simply not reproduced due to the constraints on the size step in θ used in this figure. However, it is possible to note that the values of the cost function in Figs. 4a and 5c are comparable. In all the plots presented in Fig. 5, the different combinations of θ_i's, for $i = 1, 2, 3, 4$, (plotted in the abscissas) are generated by nested loops, where the inner loop corresponds to θ_4 and the outer loop corresponds to θ_1. For instance, in Fig. 5a, case 1 corresponds to $\theta = [0\ 0\ 0\ 0]^{\mathrm{T}}$, case 2 corresponds to $\theta = [0\ 0\ 0\ -5]^{\mathrm{T}}$, and so on.

In this case, the amplitude of the sinusoidal excitation is varied according to the value of the cost function J. The amplitude a of the probing signal $a\sin(\omega k)$ (see Fig. 3) is reduced as the value of the cost function J is minimized by the extremum seeking procedure. Similar strategies are followed in all the simulation cases presented in this paper.

In order to obtain a better matching for the derivatives, we considered the case characterized by the cost function parameters

$$K_X = 2000, \quad K_Y = 1000, \quad K_X^{\mathrm{der}} = 1, \quad K_Y^{\mathrm{der}} = 1$$
$$K_X^{\mathrm{int}} = K_Y^{\mathrm{int}} = 0, \quad k_1 = 1, \quad k_2 = 1, \quad k_3 = 0. \tag{29}$$

Fig. 6 shows the extremum seeking results. The converged value of θ, and its state at $z = L_{\mathrm{m}}$, are

$$\hat{\theta}_{\mathrm{conv}} = \begin{bmatrix} 35.978 \\ -33.933 \\ 21.384 \\ -32.508 \end{bmatrix}, \quad x(L_{\mathrm{m}}) = \begin{bmatrix} 0.001070 \\ -0.006730 \\ 0.003289 \\ 0.011034 \end{bmatrix}. \tag{30}$$

Comparing $x(L_{\mathrm{m}})$ with x_{tar}, we can note that we still have very good matching for X and Y, and we improve the matching for Y' keeping an acceptable matching for X'. The question of what is "good matching" arises here. The matching quality is usually related to how the matching error propagates downstream the particle accelerator. This issue will be further discussed in the last simulation study of this section, where a periodic channel is considered to follow the matching channel. Until then, our assessment on the quality of the matching will be kept more qualitative than quantitative, simply because we do not have a real quantitative measure of "good matching."

Fig. 6c shows the beam envelope as a function of z (beam envelope trajectory) for $\theta = \hat{\theta}_{\mathrm{conv}}$. It is interesting to note that the value for $\hat{\theta}_{\mathrm{conv}}$ is very different from the one in the previous case. The time evolution of $\theta_1, \theta_2, \theta_3, \theta_4$ in Fig. 6b shows that the convergence is not as fast as in the previous case, where we only care about the matching of X and Y, but it is nevertheless very good. We can see that after 200 iteration we arrive at an acceptable solution, which improves even more with subsequent iterations. This can be also noted from Fig. 6a, where the cost function does not reach a steady value after 500 iterations. This is an indication that the result can be improved by increasing the number of iterations or possibly by changing some of the variables of the extremum seeking procedure.

Real trajectory as desired trajectory: We are interested in determining whether the extremum seeking procedure could converge to the global minimum if more information about this minimum were given. In this case we take $X_{\mathrm{des}}(z)$ and $Y_{\mathrm{des}}(z)$ as the solution of the KV equations when $\theta = [38\ -38\ 38\ -38]^{\mathrm{T}}$, the global minimum. The cost function parameters are chosen as

$$K_X = 200, \quad K_Y = 200, \quad K_X^{\mathrm{der}} = 1, \quad K_Y^{\mathrm{der}} = 1$$
$$K_X^{\mathrm{int}} = K_Y^{\mathrm{int}} = 10000, \quad k_1 = 1, \quad k_2 = 1, \quad k_3 = 1 \tag{31}$$

and the weight $w(z)$ is chosen as shown in Fig. 7a. Fig. 7 and 8 show the extremum seeking results. The converged value of θ, and its associated state at $z = L_{\mathrm{m}}$, are

$$\hat{\theta}_{\mathrm{conv}} = \begin{bmatrix} 38.028 \\ -38.025 \\ 38.123 \\ -38.011 \end{bmatrix}, \quad x(L_{\mathrm{m}}) = \begin{bmatrix} 0.001095 \\ -0.007871 \\ 0.003291 \\ 0.011725 \end{bmatrix}. \tag{32}$$

Comparing $x(L_{\mathrm{m}})$ with x_{tar}, we can note that we have very good matching. In this case we are indeed converging to $\theta = [38\ -38\ 38\ -38]^{\mathrm{T}}$, the global minimum. Fig. 8a shows the beam envelope as a function of z (beam envelope trajectory) for $\theta = \hat{\theta}_{\mathrm{conv}}$, where it is possible to note that X

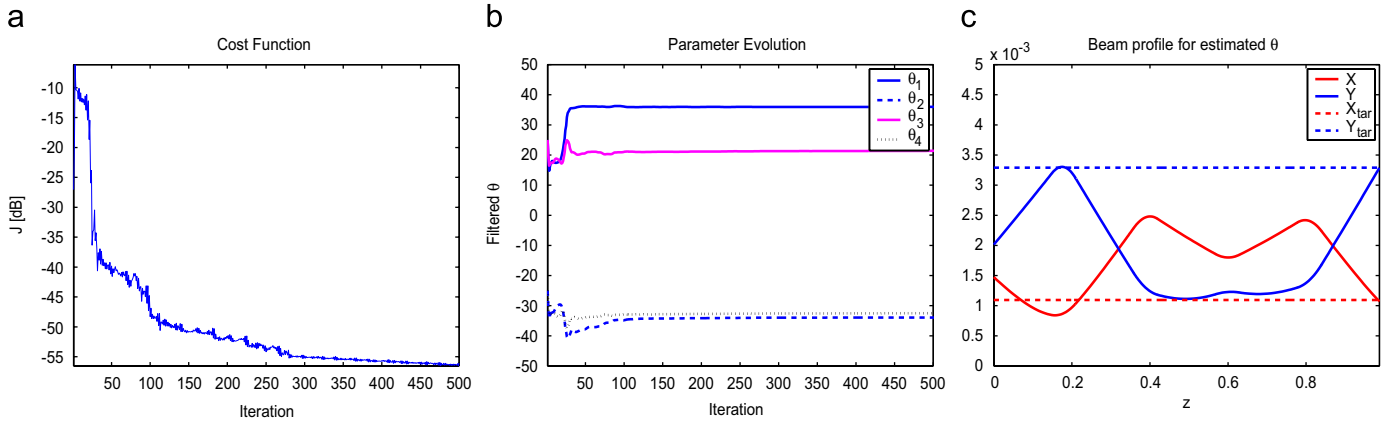

Fig. 6. (a) Cost function evolution, (b) θ evolution, and (c) beam envelope trajectory for $\theta = \hat{\theta}_{\mathrm{conv}}$.

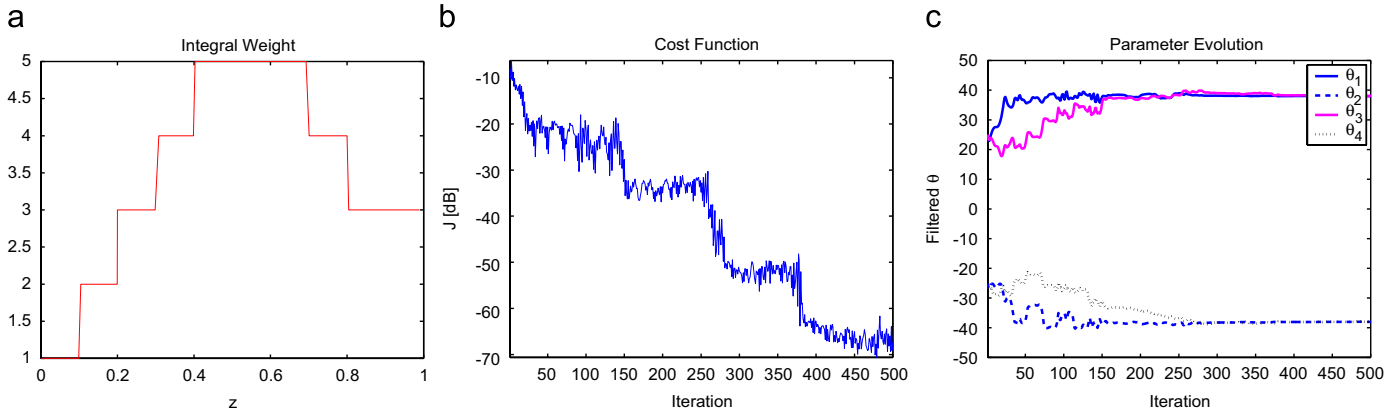

Fig. 7. (a) Integral weight, (b) cost function, and (c) θ evolution.

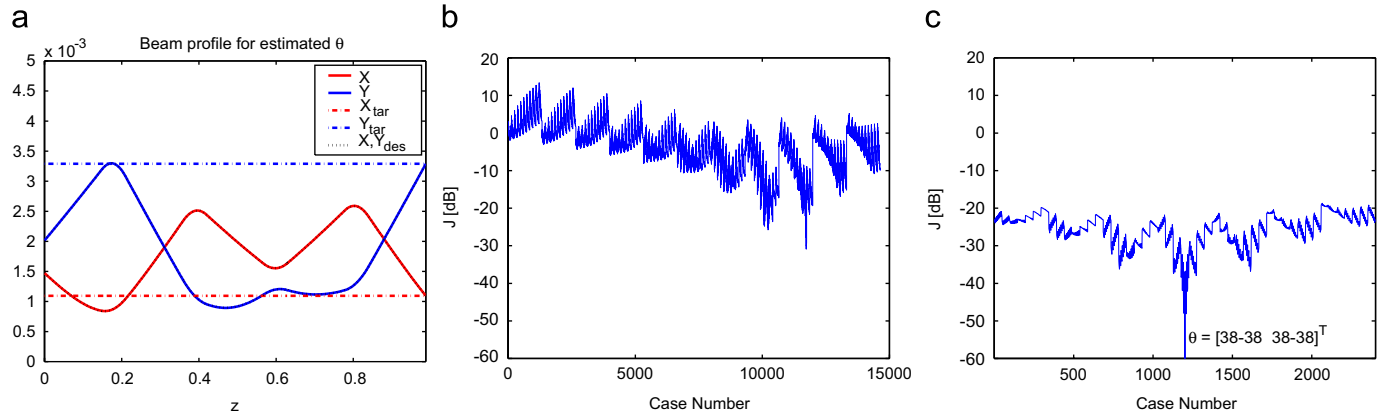

Fig. 8. (a) Beam envelope trajectory for $\theta = \hat{\theta}_{\text{conv}}$, (b) and (c) cost function map for different combinations of $\theta_1, \theta_2, \theta_3, \theta_4$.

and Y perfectly match X_{des} and Y_{des}, respectively. The time evolution of $\theta_1, \theta_2, \theta_3, \theta_4$ in Fig. 7c shows that a steady value is reached after less than 400 iterations. This can also be noted from the evolution of the cost function in Fig. 7b. This figure also shows the effect of varying $a = \text{diag}([a_1\ a_2\ a_3\ a_4])$ as a function of the value of J. It is possible to note the steps in the evolution of J thanks to the change of the sinusoidal amplitude. In this particular case, the amplitudes of the sinusoidal excitations are reduced when the cost function J decreases, according to the following law: $[a_1\ a_2\ a_3\ a_4]$ is equal to [2.25 2 1.75 1.5] if $-35\,\text{dB} \leqslant J$, [0.5 0.75 0.5 0.5] if $-40\,\text{dB} \leqslant J < -35\,\text{dB}$, [0.1 0.25 0.25 0.25] if $-50\,\text{dB} \leqslant J < -40\,\text{dB}$, [0.05 0.05 0.25 0.25] if $-60\,\text{dB} \leqslant J < -50\,\text{dB}$, [0.01 0.01 0.05 0.05] if $J < -60\,\text{dB}$. We should note that the reduction of the amplitude of the probing signal does not make the cost function J decrease, but allows it to stay around a lower local minimum value once this minimum is reached. Fig. 8 also shows the cost function plotted as a function of $\theta_1, \theta_2, \theta_3, \theta_4$. In Fig. 8b, θ_i, $i = 1, 2, 3, 4$ is varied from 0 to 50 in steps of 5. In Fig. 8c, θ_i, $i = 1, 2, 3, 4$ is varied from 35 to 41 in steps of 1. The negative peak for the case $\theta = [38\ \ -38\ \ 38\ \ -38]^{\text{T}}$ is manifested in this figure. Comparing this map with the ones corresponding to the cases with only terminal constraints we can note that the map is not as spiky, and on average (after an imaginary low-pass filter) a better parabola is described.

Double linear interpolation as desired trajectory: The trajectory of the beam envelope corresponding to the global minimum is not available in real applications. The designer is therefore required to have an intuitive understanding as to what makes a good desired beam envelope trajectory. The beam envelope will track the desired trajectory as closely as possible. These conditions lead to optimality only if the desired beam envelope trajectory is chosen properly (in an optimal sense). The choice of the desired trajectory is particularly important for under-determined systems, where the degrees of freedom (number of lenses) is strictly higher than the number of constraints (e.g., initial conditions, target conditions, maximum or minimum values of the lens strengths). In these cases the solution for the matching problem (i.e., making $x(L_{\text{m}}) = x_{\text{tar}}$) may not be unique, and the choice of the desired trajectory has a decisive influence on the outcome of the optimization procedure. In this case we take $X_{\text{des}}(z)$ and $Y_{\text{des}}(z)$ as a combination of two linear

functions as shown in Fig. 9 (dotted line). The slope of the last portion of the desired beam envelope trajectory coincides with the target conditions for the derivatives $(X'_{\rm tar}, Y'_{\rm tar})$ at $z = L_{\rm m}$ in order to avoid any type of incompatibility. The use of only one linear function, connecting $X_{\rm ini}$ and $Y_{\rm ini}$ at $z = 0$, with $X_{\rm tar}$ and $Y_{\rm tar}$ at $z = L_{\rm m}$, respectively, would be in conflict with the terminal conditions for the derivatives. Figs. 9 and 10 show the extremum seeking results when the cost function parameters are given by

$$K_X = 2000, \quad K_Y = 2000, \quad K_X^{\rm der} = 1, \quad K_Y^{\rm der} = 1$$
$$K_X^{\rm int} = K_Y^{\rm int} = 50, \quad k_1 = 1, \quad k_2 = 1, \quad k_3 = 1. \tag{33}$$

The integral weight $w(z)$ is shown in Fig. 10a. We try not only to match the final portion of the beam envelope trajectory to prescribed target values, but also to reduce excursions in the middle section. However, the former goal is priority and this is reflected in the selection of the weight function. Although not zero, the weight function for $0 < z \leqslant 0.8$ is much smaller than for $z \geqslant 0.8$. This also responds to the degree of confidence we have in the desired trajectory. Note that the linear function proposed in this case intends only to reduce excursions of the beam envelope in the middle section, but it is far from representing a feasible beam trajectory. This case is very different from the previous one (Fig. 7a), where we had a high degree of confidence in the desired trajectory (we knew that the considered desired trajectory indeed corresponded to the matching solution (global minimum)).

The converged value of θ, and its associated state at $z = L_{\rm m}$, are

$$\hat{\theta}_{\rm conv} = \begin{bmatrix} 34.855770 \\ -30.710796 \\ 14.736266 \\ -30.669086 \end{bmatrix}, \quad x(L_{\rm m}) = \begin{bmatrix} 0.001093 \\ -0.007343 \\ 0.003280 \\ 0.010630 \end{bmatrix}. \tag{34}$$

Comparing $x(L_{\rm m})$ with $x_{\rm tar}$, we can note that we do have very good matching for the final conditions. It is interesting to note how different the value of $\hat{\theta}_{\rm conv}$ is from the global minimum and at the same time how good the matching is. The time evolution of $\theta_1, \theta_2, \theta_3, \theta_4$ in Fig. 10c shows that a steady value is reached after 150 iterations. This can be also noted from Fig. 10b, where the cost function reaches a steady value after 150 iterations, showing a very fast convergence. Fig. 9 shows the beam envelope trajectory for $\theta = \hat{\theta}_{\rm conv}$. Not only the matching of the target conditions is very good, but also the matching of the desired beam envelope trajectory. This is explained by how the cost function was defined. The figure also compares the beam envelope trajectory for $\theta = \hat{\theta}_{\rm conv}$ with the beam envelope trajectory associated with the global minimum $\theta = [38 \ -38 \ 38 \ -38]^{\rm T}$. From the comparison we can conclude that we achieve very similar final conditions reducing at the same time the excursion of $X(z)$ and $Y(z)$ around the desired trajectory.

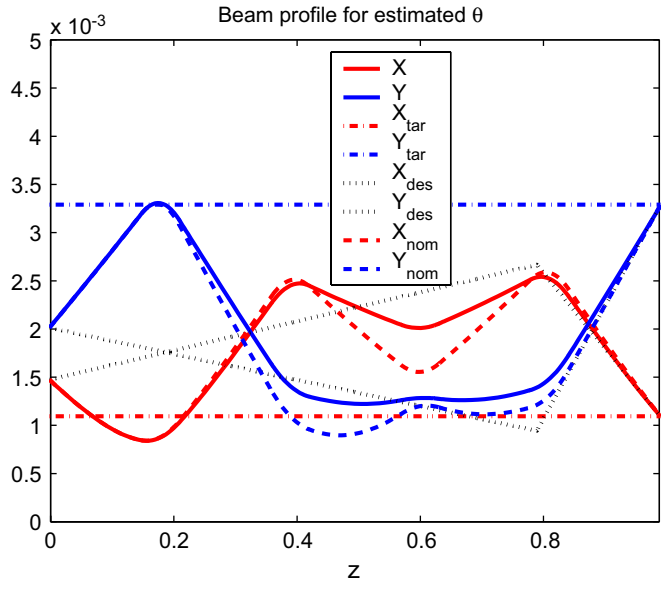

Fig. 9. Beam envelope trajectory for $\theta = \hat{\theta}_{\rm conv}$, desired beam envelope trajectory $X_{\rm des}(z)$, $Y_{\rm des}(z)$, beam envelope trajectory for $\theta = [38 \ -38 \ 38 \ -38]^{\rm T}$ (nom), and target values for X and Y at $z = L_{\rm m}$.

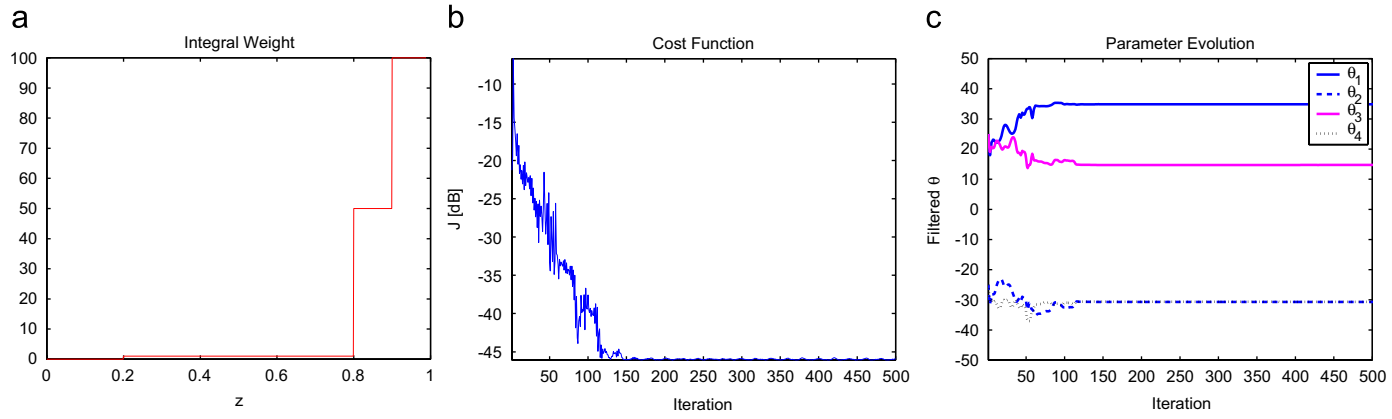

Fig. 10. (a) Integral weight, (b) cost function, and (c) θ evolution.

Target conditions at multiple locations: We consider now the following initial (entrance of the channel) and target conditions:

$$x_{\text{ini}} = \begin{bmatrix} 0.001157 \\ -0.01104 \\ 0.003239 \\ 0.000075 \end{bmatrix}, \quad x_{\text{tar}} = \begin{bmatrix} 0.001092 \\ 0 \\ 0.002055 \\ 0 \end{bmatrix} \tag{35}$$

where the target condition is specified at the center of the first quadrupole of the periodic channel, i.e., at $z = L_1$ (see Fig. 2). These specified target conditions, if achieved, ensure a periodic evolution of the beam after $z = L_1$. The initial conditions for the extremum seeking parameters are $\theta_1(0) = \theta_3(0) = 25$, and $\theta_2(0) = \theta_4(0) = -25$.

Fig. 11 shows the extremum seeking results when the cost function parameters are given by

$$K_X = 1000, \quad K_Y = 1000, \quad K_X^{\text{der}} = 10, \quad K_Y^{\text{der}} = 10$$
$$K_X^{\text{int}} = K_Y^{\text{int}} = 0, \quad k_1 = 1, \quad k_2 = 1, \quad k_3 = 0. \tag{36}$$

In this case, J_1 and J_2 are slightly modified as follows:

$$J_1 = K_X(x(L_1) - X_{\text{tar}})^2 + K_Y(Y(L_1) - Y_{\text{tar}})^2$$
$$J_2 = K_X^{\text{der}}(X'(L_1) - X'_{\text{tar}})^2 + K_Y^{\text{der}}(Y'(L_1) - Y'_{\text{tar}})^2.$$

The converged value of θ, and its associated state at $z = L_1$, are

$$\hat{\theta}_{\text{conv}} = \begin{bmatrix} 19.8043 \\ -39.4358 \\ 27.5275 \\ -19.1684 \end{bmatrix}, \quad x(L_1) = \begin{bmatrix} 0.001089 \\ -0.000077 \\ 0.002056 \\ -0.000430 \end{bmatrix}. \tag{37}$$

Comparing $x(L_1)$ with x_{tar}, we can note that we do have very good matching. Fig. 11a and b shows that after 500 iterations we arrive at an acceptable solution which improves even more with subsequent iterations (note that we have six lenses now). It can be also noted from Fig. 11a that the cost function does not reach a steady value after 800 iterations. This is an indication that the result can be improved by increasing the number of iterations or possibly by changing some of the variables of the extremum seeking procedure. Fig. 11c shows the beam envelope as a function of z (beam envelope trajectory) for $\theta = \hat{\theta}_{\text{conv}}$. Although we have good matching at $z = L_1$, we can see from this figure that the evolution of the beam within the periodic channel is probably below expectations, since an obvious mismatch develops downstream. If the beam is not matched at the transition region between accelerator sections, then the beam begins with envelope oscillations (the KV equations describe the beam envelope) representing excess energy caused by the initial mismatch. When the envelope oscillates like that we sometimes refer to it as a "mismatched beam". That is, the mismatch is indicated by the envelope oscillations downstream. This case study points out that an acceptable mismatching at one location of the channel can propagate to become an unacceptable mismatching at some other locations. It would be preferable thus to include into the cost function J the matching requirements at these other locations.

Specifying target conditions for multiple locations can help to overcome some practical limitations arising in the computation of the cost function (22). Although totally feasible in a simulated (off-line, model-based extremum seeking) environment, the computation of the components J_2 and J_3 can become cumbersome, or even impossible, in a real-time (on-line, non-model-based extremum seeking) experiment because of two practical constraints: (a) the measurement of the derivatives of the semi-axis of the envelope may not be possible, (b) measurements of the semi-axis of the beam envelope may be available only at a reduced number of locations along the channel. However, asking the semi-axis of the envelope to match specific target values at two consecutive locations may be equivalent to asking both the envelope semi-axis and their derivatives to match specific target values at one single location. In addition, the integral component of the cost function can be approximated by a sum of weighted, squared differences between the measured and desired envelope semi-axis at a finite number of locations. Therefore, components J_2 and J_3 in Eqs. (24) and (25) can be rewritten as J_1-like components (23) if target values for the envelope semi-axis are specified at multiple locations. In

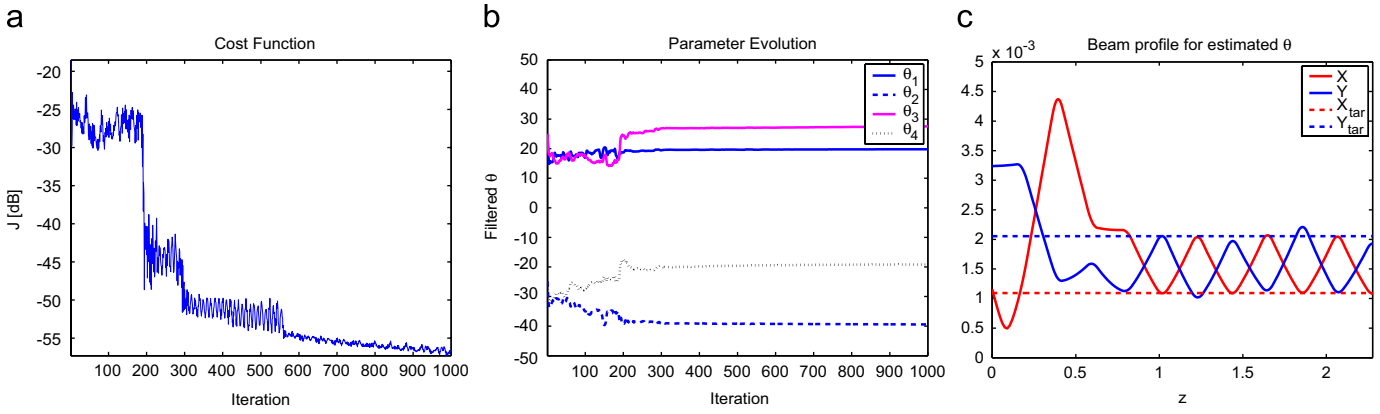

Fig. 11. (a) Cost function, (b) θ evolution, and (c) beam envelope trajectory for $\theta = \hat{\theta}_{\text{conv}}$.

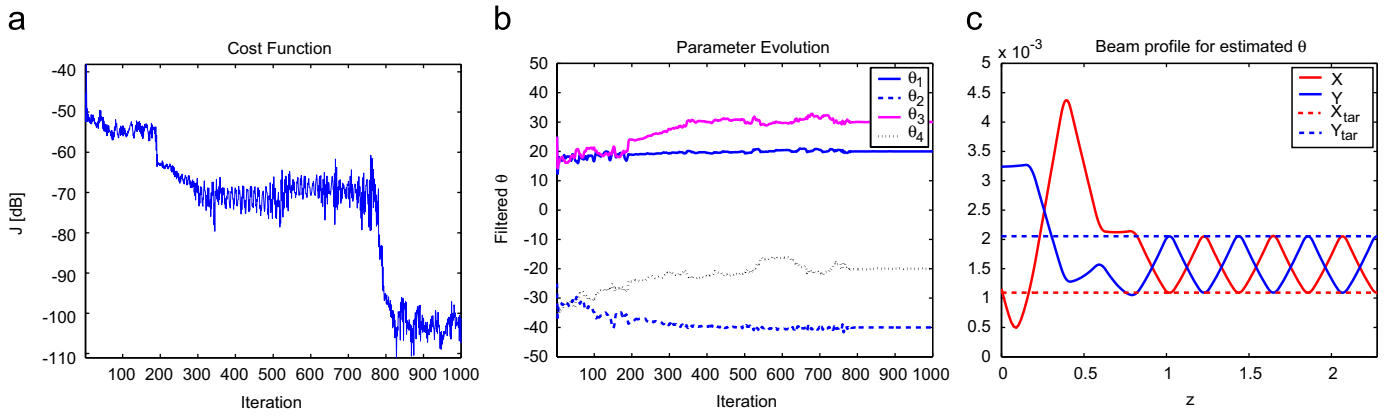

Fig. 12. (a) Cost function, (b) θ evolution, and (c) beam envelope trajectory for $\theta = \hat{\theta}_{\text{conv}}$.

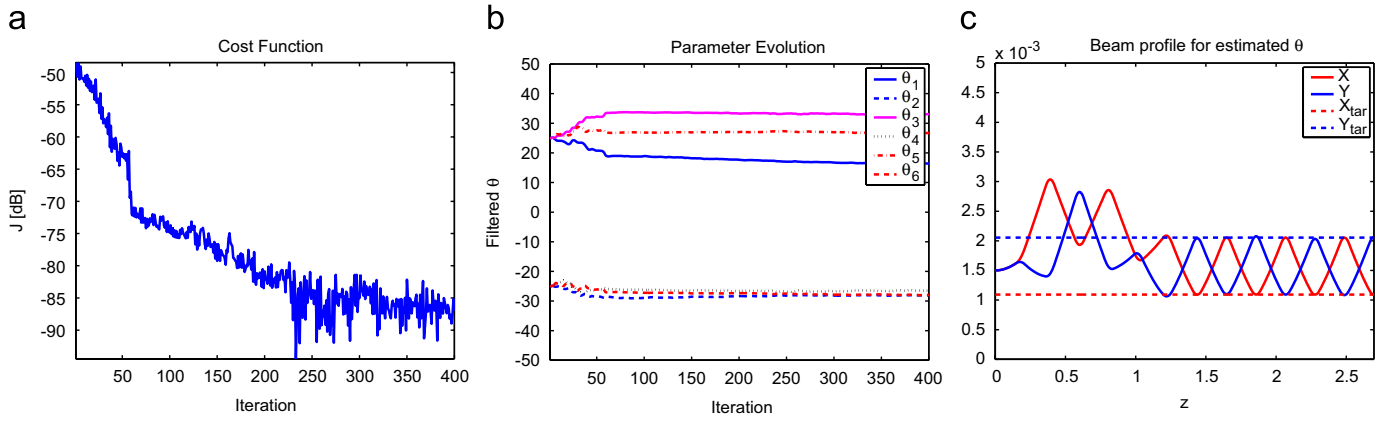

Fig. 13. (a) Cost function, (b) θ evolution, and (c) beam envelope trajectory for $\theta = \hat{\theta}_{\text{conv}}$.

this case, the cost function (22) can be computed in a real-time experiment directly from measurements of only X and Y at prescribed locations.

Fig. 12 shows the extremum seeking results when the cost function is given by

$$J = \sum_i (X(L_i) - X_{\text{tar}})^2 + (Y(L_i) - Y_{\text{tar}})^2 \tag{38}$$

where L_i, for $i = 1, 3, 5, 7$, are specific locations along the periodic channel as it is shown in Fig. 2. In this case we are replacing the derivative requirements at $z = L_1$ by multiple requirements for the beam semi-axis at different locations. We are also incorporating into the cost function discrete points of the desired trajectory within the periodic channel.

The converged value of θ, and its associated state at $z = L_1$, are

$$\hat{\theta}_{\text{conv}} = \begin{bmatrix} 19.9951 \\ -39.9986 \\ 29.9887 \\ -20.0502 \end{bmatrix}, \quad x(L_1) = \begin{bmatrix} 0.001088 \\ -0.00000765 \\ 0.002055 \\ -0.00000156 \end{bmatrix}. \tag{39}$$

Although the quality of the matching for X at $z = L_1$ decreases, the quality of the matching for both derivatives improves, and the overall matching quality within the periodic channel, which is our ultimate goal, also improves as shown in Fig. 12c.

As another example, we consider now the following initial (entrance of the channel) conditions:

$$x_{\text{ini}} = \begin{bmatrix} 0.0015 \\ 0 \\ 0.0015 \\ 0 \end{bmatrix} \tag{40}$$

and the same target conditions at $z = L_1$, which, if achieved, ensure a periodic evolution of the beam after $z = L_1$. We also consider now a six-quadrupole matching channel ($\theta = [\theta_1\ \theta_2\ \theta_3\ \theta_4\ \theta_5\ \theta_6]^{\text{T}}$). The initial conditions for the extremum seeking parameters are $\theta_1(0) = \theta_3(0) = \theta_5(0) = 25$, and $\theta_2(0) = \theta_4(0) = \theta_6(0) = -25$. Fig. 13 shows the extremum seeking results when the cost function is given by Eq. (38). The extremum seeking algorithm successfully provides a set of lens strengths in the matching channel that takes a round beam from an electron or ion

source, for instance, and matches it into a periodic lattice, where an elliptical beam is required.

5. Adaptive control

As suggested in Section 4, the extremum seeking scheme can be used for real-time optimization, taking advantage of its non-model-based nature, which represents an advantage in terms of robustness with respect to other model-based optimization techniques such as nonlinear and dynamic programming. To accelerate convergence, a hybrid scheme is envisioned, where the optimal lens strengths are computed off-line using extremum seeking, as explained in Section 4, or another optimization technique, and used as initial conditions ($\theta(0)$) for an on-line extremum seeking controller. Under this framework, the extremum seeking algorithm will be playing the role of a non-model-based adaptive controller, which is one of its unique characteristics, that ensures a well-matched beam at specified locations of the matching channel independently of the uncertainties in the system parameters.

Given $\theta_p = \theta_p^m$ (see Fig. 1), the acceptance requirement for the periodic channel, denoted x_p^m, is easily computed using numerical search algorithms. Defining $x_{tar}|_{z=L_m} = x_p^m$, the matching solution θ_i^m, for $i = 1, \ldots, 6$, that makes $x(L_m) = x_{tar}|_{z=L_m} = x_p^m$, can be computed off-line using extremum seeking in a simulated environment, as shown in the previous section, or another model-based optimization technique. Defining $\theta = [\theta_1\ \theta_2\ \theta_3\ \theta_4\ \theta_5\ \theta_6\ \theta_p]^T$, Fig. 14a shows the envelope semi-axes X and Y for the matched beam as functions of z for

$$\theta^m = [40\ \ -40\ \ 30\ \ -30\ \ 25\ \ -25\ \ 38]^T \tag{41}$$

$$x_{ini} = \begin{bmatrix} 0.002887 \\ -0.01239 \\ 0.001053 \\ 0.01292 \end{bmatrix}, \quad x_p^m = \begin{bmatrix} 0.001157 \\ -0.004266 \\ 0.001962 \\ 0.006098 \end{bmatrix}. \tag{42}$$

If θ is kept constant and equal to θ^m, Fig. 14b–d shows how the matching properties are lost when: (1) there is an actuator fault (20% increase in the strength of the third quadrupole (θ_3)), (2) there is a 50% increase for both the horizontal and vertical emittances, and (3) there is a 10% change in the initial conditions X_{ini} and Y_{ini}.

We are interested in developing a controller that can successfully cope with these changes in operation conditions, preserving the matching properties of the system, by adaptively tuning the strengths of the lenses in the matching section (and eventually in the periodic section), and minimizing a functional that is a function of the matching error.

In this section we illustrate how to use extremum seeking for adaptive tuning of θ to preserve good matching, i.e., to minimize in real time the following functional:

$$J = \{k_1 J_1 + k_2 J_2 + k_3 J_3\}^{1/2} \tag{43}$$

where k_1, k_2, k_3 are weight constants,

$$J_1 = \sum_{i=1}^{7} M_i \tag{44}$$

$$M_i = (X(L_i) - X_{tar})^2 + (Y(L_i) - Y_{tar})^2 \quad \text{for } i \text{ odd}$$
$$M_i = (Y(L_i) - X_{tar})^2 + (X(L_i) - Y_{tar})^2 \quad \text{for } i \text{ even}$$

$$J_2 = \sum_{i=2}^{7} N_i \tag{45}$$

$$N_i = (X(L_i) - X(L_1))^2 + (Y(L_i) - Y(L_1))^2 \quad \text{for } i \text{ odd}$$
$$N_i = (Y(L_i) - X(L_1))^2 + (X(L_i) - Y(L_1))^2 \quad \text{for } i \text{ even}$$
$$J_3 = (X(L_1) - X_{tar})^2 + (Y(L_1) - Y_{tar})^2 \tag{46}$$

and L_i, for $i = 1, \ldots, 7$, are specific locations along the periodic channel as it is shown in Fig. 2.

Defining J_1 as in Eq. (44) we are asking the controller to make the maxima and minima of the periodic oscillation in the periodic channel equal to prespecified values X_{tar} and Y_{tar}. Defining J_2 as in Eq. (45) we are asking the controller to make all the envelope maxima equal, and all the envelope minima equal, but without specifying values. In this way, when prespecified values X_{tar} and Y_{tar} are not achievable, at least we obtain symmetric periodic oscillations of period $2L_d + 2L_q$ in the periodic channel. The cost function component J_3 in (46) is typically used in combination with J_2 with appropriate weights to ask the controller to make the maxima and minima of the periodic oscillation achieved by J_2 be as close as possible to prespecified values X_{tar} and Y_{tar}.

For all the simulations presented in this section, the nominal initial condition, x_{ini}^n, of the beam at the entrance of the channel is that given in Eq. (42). In addition, the nominal values of the quadrupole strengths, θ^n, are equal to those given in Eq. (41). The initial conditions for the extremum seeking parameters in all the simulations are equal to the nominal values, i.e., $\theta(0) = \theta^n = \theta^m$. The target values involved in the computation of the cost function J in (43) are $X_{tar} = 0.001092$ and $Y_{tar} = 0.002055$. Below we study the performance of the extremum-seeking adaptive controller in regulating the system around the nominal beam envelope trajectory shown in Fig. 14a in the presence of faults or changes.

Actuator fault: In this case we study the response of our controller to a drift in one of the quadrupoles of the matching channel. We rewrite Eq. (20) as

$$\theta(k+1) = \frac{k}{D} d + \hat{\theta}(k+1) + a\cos(\omega(k+1)) \tag{47}$$

where D is the drift rate and the column vector d is used to correlate such drift with a specific quadrupole. In this simulation study, presented in Fig. 15, $D = 10^{-2}$ and $d = [0\ 0\ 1\ 0\ 0\ 0\ 0]^T$, indicating that the drift is present in the third quadrupole. In addition, we assume $\theta_p = 38 = \text{cte}$ (cte stands for constant), i.e., we use the extremum-seeking

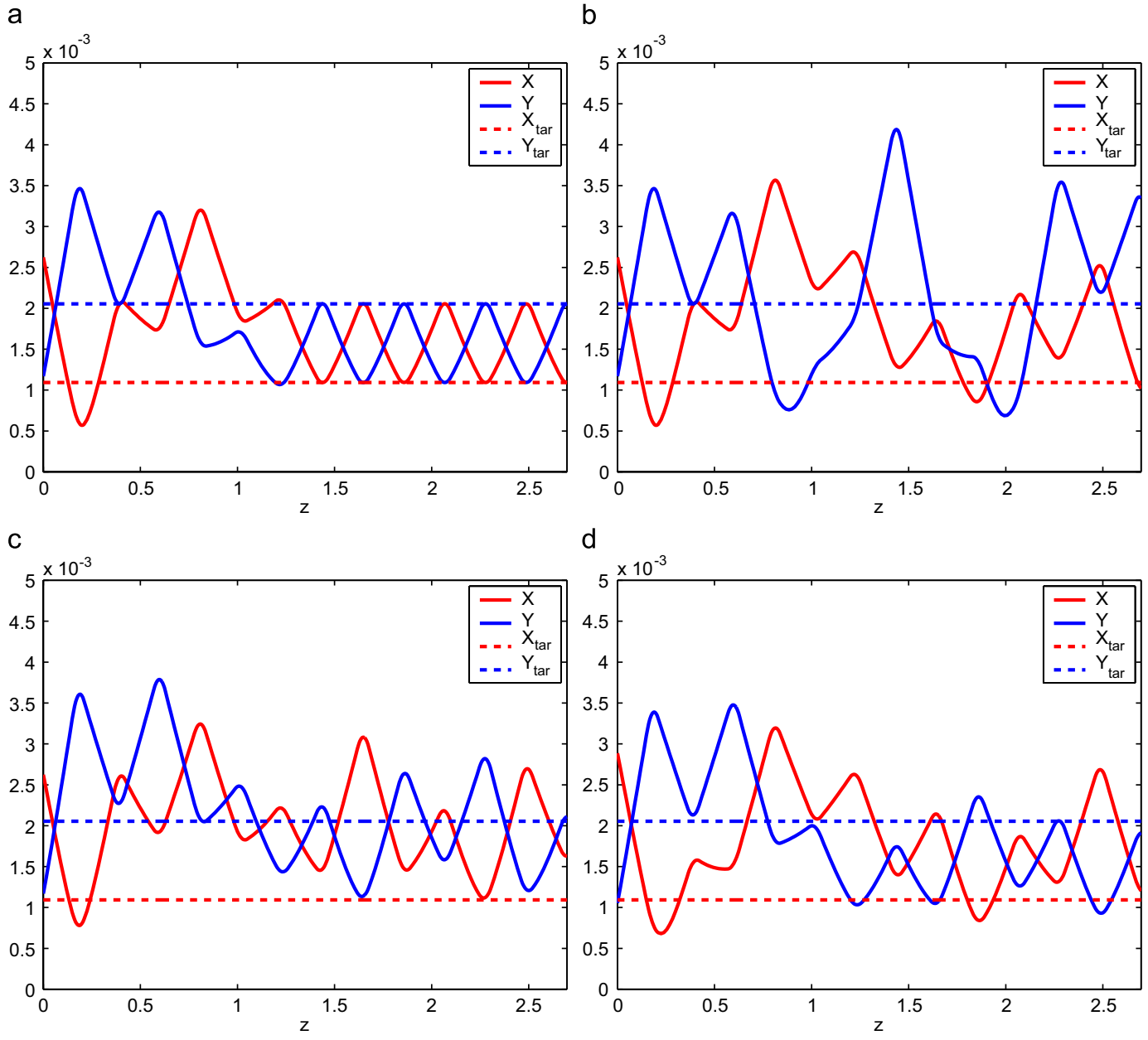

Fig. 14. Beam envelopes evolution: (a) nominal, (b) actuator fault, (c) emittance change, and (d) initial conditions change.

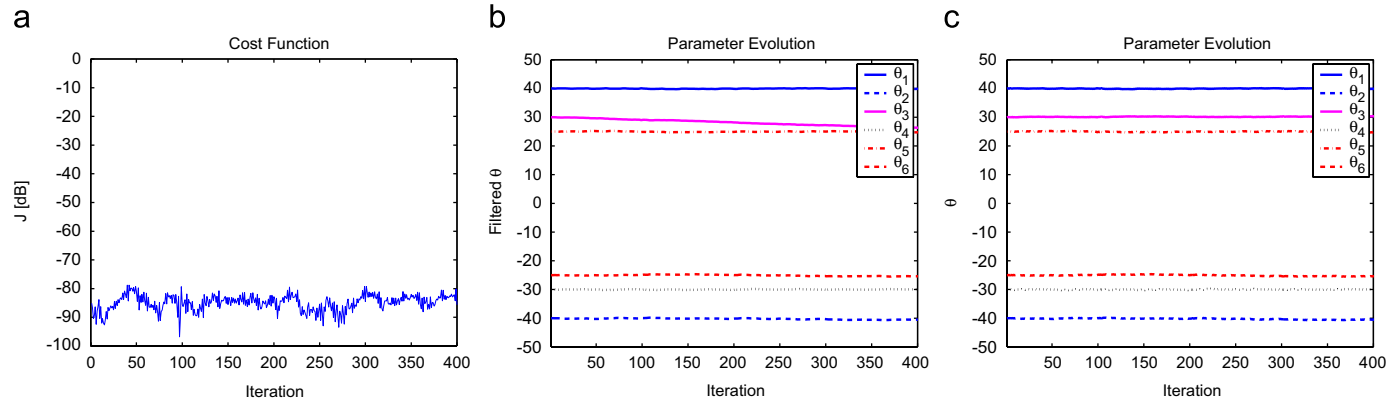

Fig. 15. Actuator drift in the third quadrupole of the matching section.

controller to tune only the strengths of the six quadrupoles in the matching channel. The controller successfully sustains the nominal beam envelope trajectory shown in Fig. 14a in spite of the actuator drift. Fig. 15a shows that the cost function (43), which was defined taking $k_1 = 1$, $k_2 = 0$ and $k_3 = 0$ in Eq. (43), is kept at its minimum run after run. This is possible due to the adaptive tuning of the quadrupole strengths θ_i, for $i = 1, \ldots, 6$. Fig. 15b shows how the outputs of the extremum seeking controller, especially the output associated with the third quadrupole ($\hat{\theta}_3$), are varied to compensate the drift, and therefore to keep θ in Fig. 15c close to its nominal value.

Initial conditions change: In this case we study the response of our controller to a change in the geometrical characteristics of the beam at the entrance of the matching section produced at the 100th run ($X_{\text{ini}} = 1.1X^n_{\text{ini}}$ and $Y_{\text{ini}} = 0.9Y^n_{\text{ini}}$). This change in initial conditions may be produced by a fault in the preceding section of the accelerator. In this simulation study, presented in Fig. 16, we again assume $\theta_p = 38 = \text{cte}$, i.e., we use the extremum-seeking controller to tune only the strengths of the six quadrupoles in the matching channel. The cost function (43), whose evolution is shown in Fig. 16a, is also defined here taking $k_1 = 1$, $k_2 = 0$ and $k_3 = 0$ in (43). Fig. 16a shows through the sudden increase in the value of the cost function at the 100th run how the matching properties of the system are transitorily lost. This can be also noted by comparing Fig. 16b and c, showing the beam envelope trajectory before and after the change in initial conditions. The controller successfully recovers the matching properties after the transient, as it is shown in Fig. 16e, by adaptively tuning the strengths of the quadrupoles in the matching channel (Fig. 16d). Fig. 16f shows the matched beam envelope trajectory before and after the change in initial conditions. It is possible to note how the beam envelope trajectory within the matching section is changed by the controller in order to preserve the characteristics of the beam envelope trajectory in the periodic section.

Emittance change: In this case we study the response of our controller to a positive change of 50% in the emittance of the beam produced at the 100th run ($\varepsilon_X = 9 \times 10^{-6}$, $\varepsilon_Y = 9 \times 10^{-6}$). In this simulation study, presented in Fig. 17, we again assume $\theta_p = 38 = \text{cte}$, i.e., we use the extremum-seeking controller to tune only the strengths of the six quadrupoles in the matching channel. The cost function (43), whose evolution is shown in Fig. 17a, is now defined taking $k_1 = 0$, $k_2 = 1$ and $k_3 = 0$ in Eq. (43). This is motivated by the fact that given the properties of the beam (emittance and perveance) and fixed strength θ_p of the quadrupoles in the periodic channel, it is not always possible to achieve arbitrary values of X_{tar} and Y_{tar} (desired minimum and maximum of the symmetric beam envelope trajectory in the periodic channel). Under these circumstances, the symmetry of the beam is prioritized over

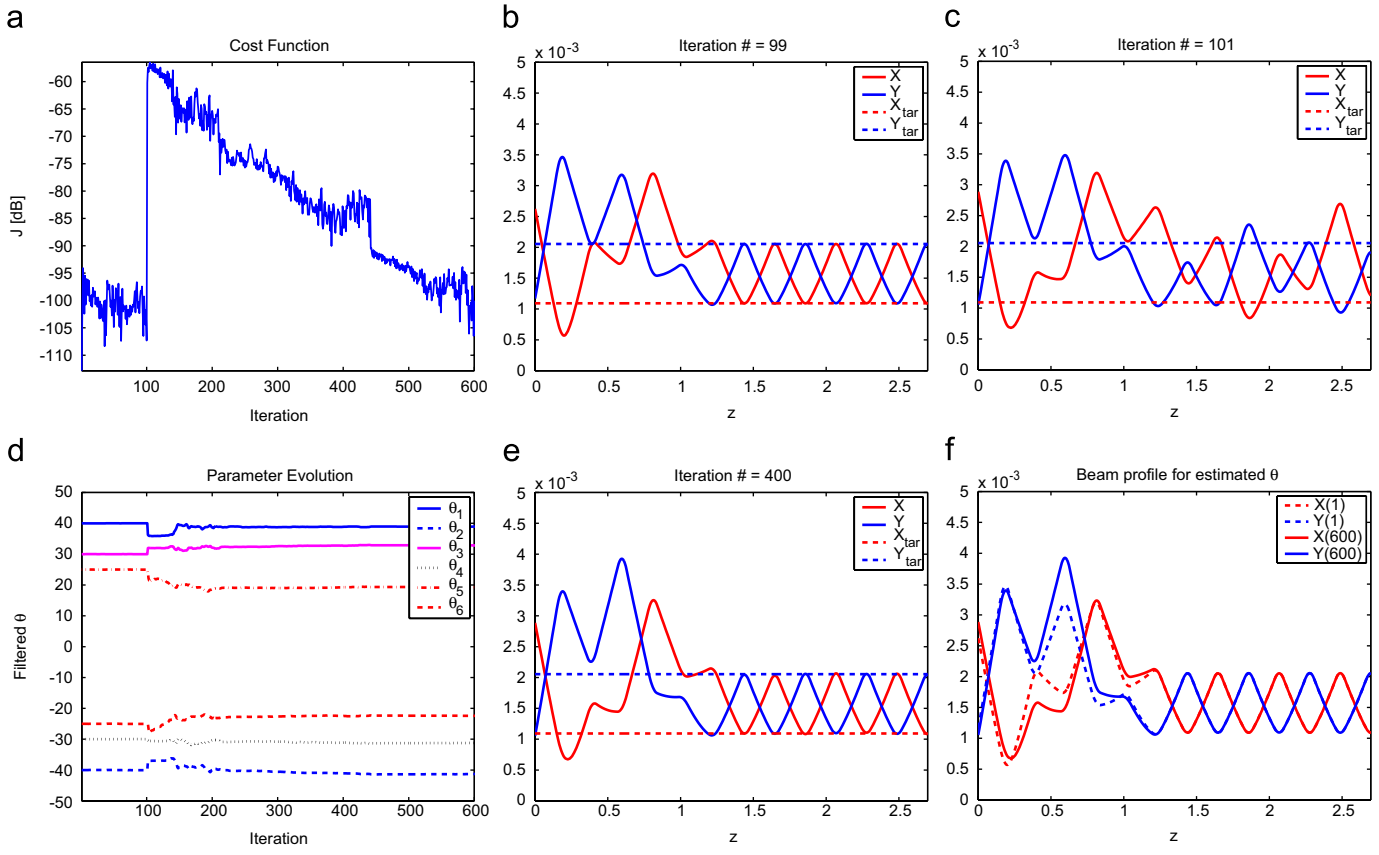

Fig. 16. Change of geometrical characteristics of the beam at the entrance of the matching channel at the 100th iteration.

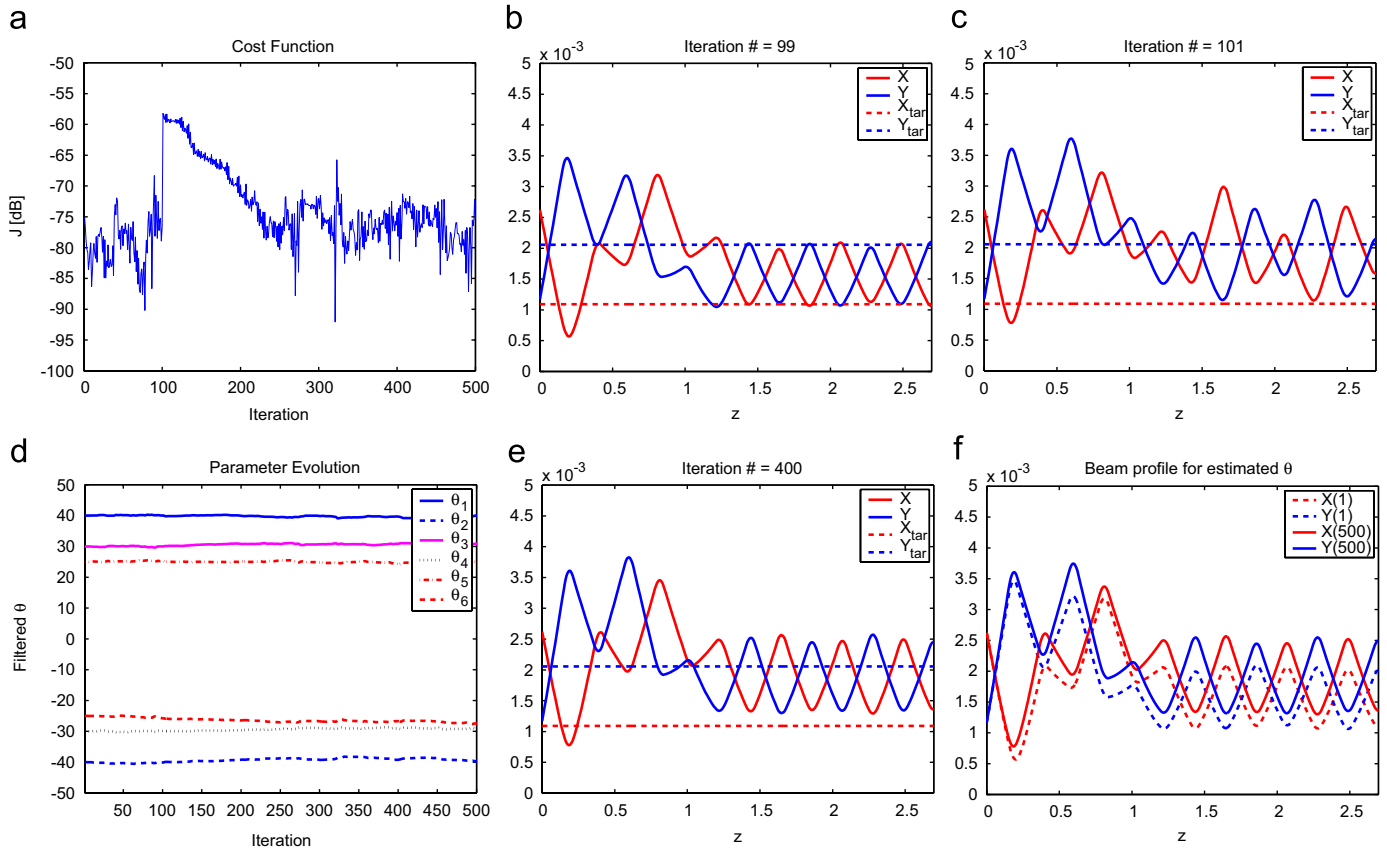

Fig. 17. Change of emittance of the beam at the 100th iteration.

its geometrical dimensions as it is reflected by the definition of the cost function J. Basically, we give to the system one more degree of freedom to accommodate the change in the properties of the beam (emittance). Fig. 17a shows through the sudden increase in the value of the cost function at the 100th run how the matching properties of the system are lost transitorily. This can be also noted by comparing Fig. 17b and c, showing the beam envelope trajectory before and after the change in emittance. By adaptively tuning the strengths of the quadrupoles in the matching channel, as shown in Fig. 17d, the controller successfully recovers the matching properties after the transient (Fig. 17e). However, in this case only the "shape", and not the "value", of the beam envelope trajectory can be preserved within the matching section. Fig. 17f shows the regulated beam envelope trajectory before and after the change in emittance. In this case, not only the beam envelope trajectory within the matching section must be changed by the controller, but also the size of the beam within the periodic section, in order to guarantee symmetry of the beam (maxima of X and Y are identical, minima of X and Y are identical).

Multiple faults or changes: In this case we consider simultaneous fault or change occurrences. At the 100th run, a 10% change in the third quadrupole of the matching section, a 10% change in the geometrical characteristics of the beam at the entrance of the matching section ($X_{\text{ini}} = 1.1X^n_{\text{ini}}$ and $Y_{\text{ini}} = 0.9Y^n_{\text{ini}}$), and a 50% change in the emittance of the beam produced ($\varepsilon_X = 9 \times 10^{-6}$, $\varepsilon_Y = 9 \times 10^{-6}$) are simulated. The cost function (43), whose evolution is shown in Fig. 18a, is now defined taking $k_1 = 0$, $k_2 = 1$ and $k_3 = 0.1$ in Eq. (43). This selection ($k_1 = 0$, $k_2 \neq 0$) is motivated by the fact that given the properties of the beam (emittance and perveance), and fixed the initial conditions of the beam x_{ini}, it is not always possible to achieve arbitrary values of X_{tar} and Y_{tar} (desired minimum and maximum of the symmetric beam envelope trajectory in the periodic channel). Under these circumstances, as it was done in the previous case, the symmetry of the beam is prioritized over its geometrical measures, as it is manifested in the definition of the cost function J. In this simulation study, presented in Fig. 18, we do not assume $\theta_p = \text{cte}$, i.e., we use the extremum-seeking controller to tune not only the strengths of the six quadrupoles in the matching channel but also the common strength of the quadrupoles in the matching section. The goal is to use the extra parameter $\theta_7 = \theta_p$ in the extremum seeking controller to make the size of the beam as close as possible to that defined by X_{tar} and Y_{tar} ($k_3 \neq 0$). Fig. 18a shows through the sudden increase in the value of the cost function at the 100th run how the matching properties of the system are lost transitorily. This can be also noted by comparing Fig. 18b and c, showing the beam envelope trajectory before and after the multiple

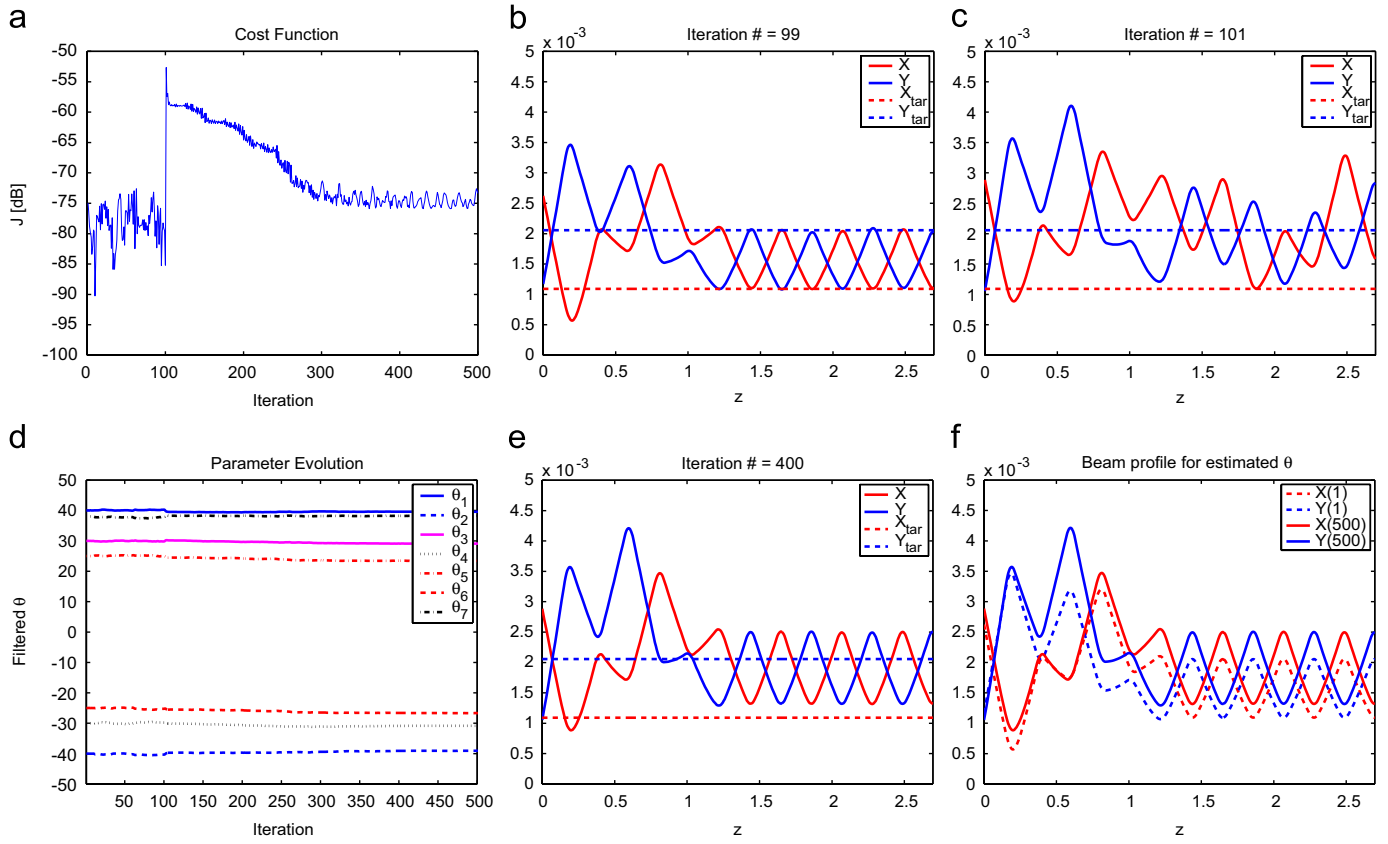

Fig. 18. Multiple faults or changes at the 100th iteration: actuator step in the third quadrupole, change in the initial conditions and emittance of the beam.

changes. In addition, Fig. 18a shows how the system is driven from a minimum before the changes at the 100th run to another different minimum after a transient that follows the changes. By adaptively tuning the strengths of the quadrupoles in both the matching and the periodic channels, as shown in Fig. 18d, the controller successfully recovers the matching properties after the transient (Fig. 18e). However, in this case only the "shape", and not the "value", of the beam envelope trajectory can be preserved within the periodic section. We must emphasize that this is not a constraint of the controller but of the system itself. Fig. 18f shows the matched beam envelope trajectory before and after the multiple changes. In this case, not only the beam envelope trajectory within the matching section must be changed by the controller, but also the size of the beam within the periodic section, in order to guarantee symmetry of the beam (maxima of X and Y are identical, minima of X and Y are identical).

6. Conclusions

Extremum-seeking has been proved to be an effective optimization technique to find an optimally matched solution. Although no limitation in terms of convergence to a (at least local) minimum is envisioned, no benefit over other optimization techniques can be claimed when the extremum-seeking algorithm is implemented *off-line*. Indeed, in some cases the convergence time can be larger than those associated with model-based techniques, where more information of the system, i.e., the model, is exploited. However, the unique characteristic of the extremum seeking algorithm is the possibility of being implemented *on-line*, which transforms this optimization technique into an adaptive control algorithm.

A multi-parameter, extremum-seeking, non-model-based, adaptive controller has been designed, and successfully tested in simulations, for the tuning of the lens strengths in four-lens and six-lens matching channels combined with a periodic channel. Based on the promising results obtained in the simulation study, it is anticipated that the scheme can play an important role in real-time adaptive control of beam envelopes in particle accelerators. Due to its non-model-based nature, which represents an advantage with respect to other model-based optimization techniques, the extremum-seeking controller can cope with model uncertainties and system errors, faults, or changes.

Another unique property of this type of controller is the flexibility that the designer has to define control goals by the appropriate definition of the cost function J. Due to this flexibility, constraints of the system as well as competing objectives can be introduced into the controller. Future work by the authors will include the development of analytical expressions for sensitivity of the matched beam (against "errors" in the actuators (quadrupoles)) that can

be incorporated into the extremum-seeking adaptive controller functional in order not only to converge to a matching solution but also to converge to the least sensitive one (if the degrees of freedom allow it). The incorporation of sensitivity information into the cost function may represent a tradeoff between performance and robustness because it may require the use of the model, which has not been used for the cost functions considered in this work.

References

[1] S. Lund, B. Bukh, Phys. Rev. ST Accelerators Beams 7 (024801).
[2] S. Bernal, H. Li, R. Kishek, B. Quinn, M. Walter, M. Reiser, P. O'Shea, C.K. Allen, Phys. Rev. ST Accelerators Beams 9 (064202).
[3] C. Allen, M. Reiser, Nucl. Instr. and Meth. 384 (1997) 322.
[4] C. Chang, E. Horowitz, M. Reiser, Conceptual design of an electrostatic quadrupole transport system for high-brightness H-beams, in: Proceedings of the SPIE Conference on Intense Microwave and Particle Beams, vol. 1226, 1990, pp. 483–498.
[5] I. Kapchinskij, V. Vladimirskij, in: Proceedings of the International Conference on High-Energy Accelerators and Instrumentation, CERN, 1959, pp. 274–288.
[6] M. Reiser, Theory and Design of Charged-Particle Beams, Wiley, New York, 2004.
[7] M. Krstic, H.-H. Wang, Automatica 36 (4) (2000) 595.
[8] M. Rotea, Analysis of multivariable extremum seeking algorithms, in: Proceedings of the American Control Conference, vol. 1, 2000, pp. 433–437.
[9] K. Ariyur, M. Krstic, Real-Time Optimization by Extremum Seeking Feedback, Wiley, New York, 2003.
[10] P. Binetti, K. Ariyur, M. Krstic, F. Bernelli, J. Guidance Control Dyn. 26 (1) (2003) 132.
[11] J.-Y. Choi, M. Krstic, K. Ariyur, J. Lee, Tuning of a combustion controller by extremum seeking: a simulation study, in: Proceedings of the 39th IEEE Conference on Decision and Control, vol. 5, 2000, pp. 5219–5223.
[12] A. Banaszuk, K. Ariyur, M. Krstic, C. Jacobson, Automatica 40 (11) (2004) 1965.
[13] H.-H. Wang, S. Yeung, M. Krstic, IEEE Trans. Control Systems Technol. 8 (2) (2000) 300.
[14] A. Banaszuk, S. Narayanan, Y. Zhang, Adaptive control of flow separation in a planar diffuser, in: Proceedings of the 41st Aerospace Sciences Meeting & Exhibit, 2003 AIAA–2003–0617.
[15] K. Ariyur, M. Krstic, Slope seeking and application to compressor instability control, in: Proceedings of the IEEE Conference on Decision and Control, vol. 4, 2002, pp. 3690–3697.
[16] K. Peterson, A. Stefanopoulou, Automatica 40 (6) (2004) 1063.
[17] Y. Li, M. Rotea, G.-C. Chiu, L. Mongeau, I.-S. Paek, IEEE Trans. Control Systems Technol. 13 (8) (2005) 527.
[18] H.-H. Wang, M. Krstic, G. Bastin, Int. J. Adaptive Control Signal Process. 13 (1999) 651.
[19] J.-Y. Choi, M. Krstic, K. Ariyur, J. Lee, IEEE Trans. Automat. Control 47 (2) (2002) 318.
[20] G. Franklin, J. Powell, M. Workman, Digital Control of Dynamic Systems, third ed., Addison-Wesley, Reading, MA, 1997.
[21] G. Franklin, J. Powell, A. Emami-Naeini, Feedback Control of Dynamic Systems, fifth ed., Prentice-Hall, Englewood Cliffs, NJ, 2005.